Simulated Trapping of Solar Energetic Protons for the 8-10 March 2012 Geomagnetic Storm: Impact on Inner Zone Protons as Measured by Van Allen Probes

Mary K. Hudson[1,2], Miles A. Engel[3], Brian T. Kress[4], Zhao Li[1], Maulik Patel[1] and Richard S. Selesnick[5]

[1] *Physics and Astronomy Dept., Dartmouth College, Hanover, NH, USA*
[2] NCAR *High Altitude Observatory, Boulder, CO, USA*
[3]*Los Alamos National Laboratory, Los Alamos, NM, USA*
[4]*Center for Cooperative Research in the Environmental Sciences at CU Boulder, Boulder, CO, USA*
[5]*Space Vehicles Directorate, Air Force Research Laboratory, Kirtland AFB, NM, USA*

Corresponding author: Mary K. Hudson (mary.k.hudson@dartmouth.edu)

Key Points:

- Solar Energetic Proton (SEP) trapping explains double-peaked inner zone structure observed by Van Allen Probes
- Highest flux SEP event of Solar Cycle 24 produces trapping following arrival of a CME shock in March 2012
- MHD-test particle simulations followed by radial diffusion produce phase space density consistent with observed value at L ~ 2

Abstract

Solar Energetic Protons (SEPs) have been shown to contribute significantly to the inner zone trapped proton population for energies < 100 MeV and L > 1.3 (Selesnick et al., 2007). The Relativistic Electron Proton Telescope (REPT) on the Van Allen Probes launched 30 August 2012 observed a double-peaked (in L) inner zone population throughout the 7-year lifetime of the mission. It has been proposed that a strong SEP event accompanied by a CME-shock in early March 2012 provided the SEP source for the higher L trapped proton population, which then diffused radially inward to be observed by REPT at L ~ 2. Here, we follow trajectories of SEP protons launched isotropically from a sphere at 7 Re in 15s cadence fields from an LFM-RCM global MHD simulation driven by measured upstream solar wind parameters. The timescale of the interplanetary shock arrival is captured, launching a magnetosonic impulse propagating azimuthally along the dawn and dusk flanks inside the magnetosphere, shown previously to produce SEP trapping. The MHD-test particle simulation uses GOES proton energy spectra to weight the initial radial profile required for the radial diffusion calculation over the following two years. GOES proton measurements also provide a dynamic outer boundary condition for radial diffusion. A direct comparison with REPT measurements 20 months following the trapping event in March 2012 provides good agreement with this novel combination of short-term and long-term evolution of the newly trapped protons.

1. Introduction

The Earth's inner radiation belt includes a population of high-energy protons (10 MeV to 1 GeV) trapped by the geomagnetic field below altitudes ~10^4 km. The Combined Release and Radiation Effects Satellite (CRRES) provided the first detailed inner belt proton measurements near the geomagnetic equatorial plane, where the trapped population at all pitch angles is accessible (Gussenhoven et al., 1996), followed next by the launch of the Van Allen Probes two solar cycles later in 2012 (Mauk et al., 2012). Low-altitude satellites have provided a limited view of trapped protons near the loss cone and Solar Energetic Protons at high latitudes (Looper et al., 1998), impulsively accelerated in solar flares and by interplanetary shocks driven by Coronal Mass Ejections (CMEs).

The sources of inner belt protons are cosmic ray albedo neutron decay (CRAND) and Solar Energetic Protons (Selesnick et al., 2007; 2010). The CRAND mechanism has been well studied, less so the trapping of SEPs (Selesnick et al., 2014). Other significant processes, such as radial diffusion and loss during magnetic storms, have been modeled empirically with recent improvements using additional constraints from Van Allen Probes measurements (Selesnick and Albert, 2019; Engel et al., 2016). Theoretical modeling of the inner belt has included several free parameters adjusted to match the limited available data (Vacaresse et al., 1999; Selesnick et al., 2007; 2016; Selesnick and Albert, 2019). Detailed new measurements from Van Allen Probes of both the untrapped SEP population which penetrates into around L ~ 4 and the trapped proton distribution at > 18.5 MeV are of great value in constraining both the empirical and theoretical models, and in testing theories of inner belt source, loss, and transport processes.

Over seven years of measurements of the SEP source population and inner radiation belt protons are available from NASA's twin Van Allen Probes (formerly Radiation Belt Storm Probes, or RBSP), launched 30 August, 2012 (Mauk et al., 2012) and operated through 19 July 2019 (RBSP-B) and 18 October 2019 (RBSP-A). The two satellites operated in similar elliptical, near-equatorial plane orbits, carrying instrumentation of identical design, with the exception of the Magnetic Electron Ion Spectrometer (MagEIS) Proton Telescope on the Van Allen Probe B spacecraft only which nominally measures 2 - 20 MeV protons (Blake et al., 2013). More energetic proton data with high resolution in kinetic energy (~20 to 76 MeV), pitch angle, and magnetic L shell are available from the Relativistic Electron Proton Telescope (REPT) (Baker et al., 2012) with higher energies measured by the Relativistic Proton Spectrometer (RPS) from 50 MeV to 2 GeV (Mazur et al., 2013). Additionally, new tools have been developed to model the long timescale evolution of the inner zone (Selesnick et al., 2007; Selesnick and Albert, 2019), which includes variations in the Earth's magnetic field over many solar cycles as well as solar cycle variations in the atmosphere (Bregou et al., 2022). These determine loss rates at low altitudes and much shorter timescale variations in both SEP flux and the Earth's external magnetic field modified by solar activity. SEP cutoff models which calculate the penetration of SEPs to low altitudes using both empirical (Smart and Shea, 2009; Kress et al., 2010; 2013; 2015) and MHD fields driven by measured solar wind input at L1 (Kress et al., 2004; 2010) have been advanced. These have recently been tested against near-equatorial plane measurements (Qin et al., 2018; Li et al., 2021), along with modeling the outer boundary of trapped protons (Engel et al., 2016), using observations from the Van Allen Probes.

In earlier work, we analyzed 27 - 45 MeV proton measurements from Highly Elliptical Orbiting (HEO) satellites and showed that both enhancement and loss of inner zone protons can result

from CME-shock driven storms (Selesnick et al., 2010). Enhancement is correlated with the level of SEP flux and loss correlated with the magnitude of magnetic field perturbation associated with buildup of the storm time ring current parametrized by the Dst index. Loss was modeled and compared with REPT measurements by Engel et al. (2016) for the 17 March 2015 storm, while SEP cutoffs were modeled and compared with REPT measurements for the 11 September 2017 non-storm SEP event (Qin et al., 2019) and the 5-9 September 2017 SEP event accompanied by a strong geomagnetic storm (Li et al., 2021).

Event studies facilitate model comparison with observations on shorter time scales than the long term inner zone model developed by Selesnick et al. (2007) and extended by Selesnick and Albert (2019), comparing with REPT measurements. While the current solar maximum has not provided SEP events of the magnitude seen during the previous solar cycle (Hudson et al., 2004; Selesnick et al., 2010; Mazur et al., 2006), REPT has measured SEPs accompanying numerous moderate CME-shocks, with extraordinary energy and pitch angle resolution compared to prior available data sets.

This paper seeks to understand how trapping occurs, since only a subset of SEP events produce trapping (Selesnick et al., 2010). Earlier studies have shown that SEP trapping results from CME-shock compression of the dayside magnetopause (Hudson et al., 1997; Kress et al., 2005) without resolving whether it is the changed magnetic field configuration or accompanying inductive electric field which produces the trapping. Solar Cycle 24 was a particularly weak maximum by all measures, including the number and magnitude of SEP events ftp://ftp.swpc.noaa.gov/pub/indices/SPE.txt), with the strongest in terms of Proton Flux Units (protons/cm^2-s-sr) of > 10 MeV protons at GOES reaching 6,550 pfu on 7 March 2012, as compared with 29,500 pfu on 29 October 2003 (the so-called Halloween storm interval of Solar Cycle 23) and a maximum of 210 pfu on 5 September 2017, to contrast the range of SEP events for which trapping has been observed (Selesnick et al., 2010; Mazur et al., 2006; Hudson et al., 2021). The Relativistic Electron Proton Telescope (REPT) on the Van Allen Probes observed a double-peaked (in L) inner zone population throughout the 7-year lifetime of the mission (Baker et al., 2021, Figure 50). It has been proposed that a strong SEP event accompanied by a CME-shock in early March 2012 provided the SEP source for the higher L trapped proton population seen by Van Allen Probes (Selesnick et al., 2016), which then diffused radially inward to be observed at $L \sim 2$.

In the present study, we follow trajectories of SEP protons launched isotropically from a sphere at 7 Re in 15s cadence electric and magnetic fields from global MHD simulations driven by upstream solar wind parameters measured at L1. The simulations capture the timescale of the interplanetary shock arrival and launch of a magnetosonic impulse in magnetic and electric field components B_z and E_φ, propagating azimuthally along the dawn and dusk flanks inside the magnetosphere. This impulse type has been shown previously to produce SEP trapping (Hudson et al., 1997). The MHD-test particle simulation which incorporates GOES 13 and 15 proton energy spectra for flux weighting is used to provide the initial radial profile required for a radial diffusion calculation over the following 2 years. A radial diffusion code developed by Li et al. (2017) was used to study the long-term evolution of the trapped SEP population with the diffusion coefficient implemented by Selesnick and Albert (2019). GOES proton measurements also provide a dynamic outer boundary condition for the radial diffusion calculation. A direct comparison with REPT measurements in November 2013 following the trapping event in March

2012 provides a test of this model combination of short-term and long-term evolution of the newly trapped protons.

In this study we follow a brief discussion in Section 2 of REPT observations of the 7-8 September 2017 trapping event, for which REPT measurements were available before, during and after trapping, with description of the observations available and models used to simulate the stronger 8 March 2012 trapping event in Sections 3 and 4. A comparison of the two-timescale simulation results with REPT measurements follows for November 2013 with a discussion of results and conclusions in Section 5.

2. 5 - 9 September 2017 SEP trapping event

The 5 - 9 September 2017 SEP event (Filwett et al., 2020; Kress et al., 2021; Li et al., 2021) is noteworthy as the only trapping event identified during the 7 years of Van Allen Probes measurements (Hudson et al., 2021), from the beginning of the SEP event until its merger with the inner zone. **Figure 1** shows four consecutive days 6 – 9 September 2017 of Van Allen Probes REPT measurements for the 19.3 – 23.7 MeV channel at different pitch angles (or B/B_0) indicated by color. Both A and B spacecraft data are plotted in each panel and the locations of the two spacecraft (red and blue) and GOES 16 are shown in the bottom panels at 2300 UT on 7 September, around the time of the CME-shock arrival. Strong compression of the dayside magnetopause occurred on 7 September (Li et al., 2021, Figure 6). Inward transport of untrapped SEPs as measured by spacecraft A and B at different dayside locations is observed on 7 September in the second panel of Figure 1. The resulting trapping at L ~ 3 is evident in the third panel by 8 September with some loss due to buildup of the ring current (Selesnick et al., 2010; Engle et al., 2016) evident by 9 September in the fourth panel. The higher flux for $B/B_0 = 1$ (90 degree equatorial pitch angle, red) indicates a trapped population. Notable in all four panels is the double peaked inner zone structure, with peaks near L = 1.5 and 2, which persisted throughout the 7 years of Van Allen Probes observations (Baker et al., 2021, Figure 50). The September 2017 SEP trapping event observed in Figure 1 is seen to be weaker by three orders of magnitude than the earlier event postulated to have caused the inner zone peak seen at L = 2. Attempts to simulate the much weaker trapping event were not successful, so the remainder of this paper focuses on an earlier much stronger SEP trapping event which occurred in March 2012.

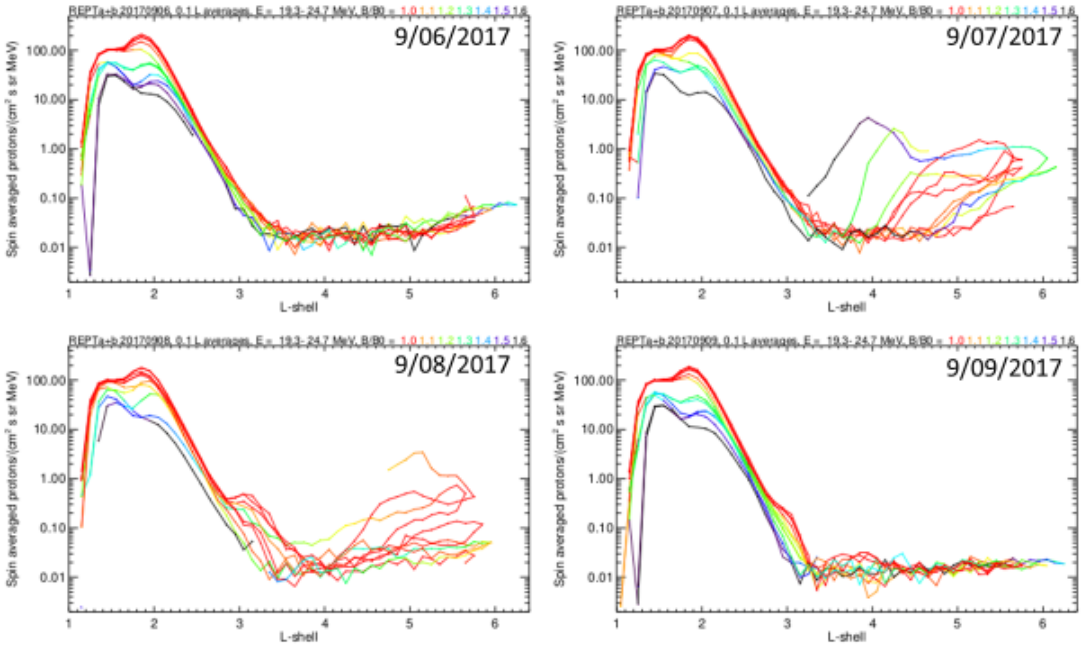

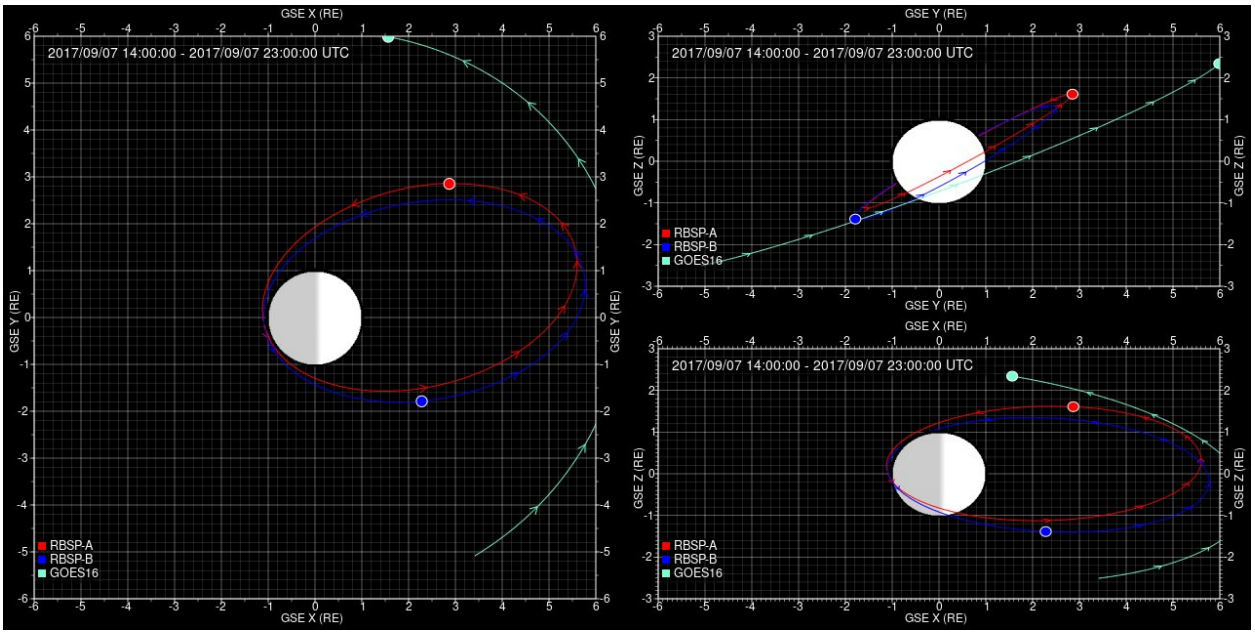

Figure 1. (Top) Plots of flux of 19.3 – 24.7 MeV protons vs. L at different equivalent equatorial pitch angles B/B0) on 6-9 September, before, during and after the trapping event which occurred during the 5 – 9 September 2017 SEP event. (Bottom) Locations of the two Van Allen Probes and GOES 16 are shown at 2300 UT on 7 September 2017.

3. 8 March 2012 SEP trapping event: MHD-test particle simulation

In this section we model a much stronger SEP trapping event (in terms of GOES > 10 MeV proton flux, 6,550 pfu on 8 March 2012 vs. 210 pfu on 5 September 2017), prior to the launch of Van Allen Probes, which Selesnick et al. (2016) have suggested may have produced the peak at L ~ 2 seen in **Figure 1**, persisting throughout the Van Allen Probes era (Baker et al., 2021, Figure 50). **Figure 2** shows both solar wind conditions from OMNIWeb and the proton flux at geosynchronous over four days of this SEP event. The GOES-13 Energetic Particle Sensor (EPS) measured 1–900 MeV proton fluxes shown in the bottom panel. The top panels plot solar wind parameters used as input to the MHD simulation described below, geomagnetic indices SymH and AE and the magnetopause location calculated using the Shue et al. (1998) model. The arrival of a CME shock at L1 propagated to the bow shock (King and Papitashvili, 2005; available at CDAWeb: https://cdaweb.gsfc.nasa.gov/index.html/) is seen ~ 1100 UT on 8 March. A strong increase in solar wind dynamic pressure Pdyn and increased positive IMF Bz is seen at this time, with subsequent strongly negative IMF Bz driving the main phase of the storm and minimum SymH = - 150 nT (third panel) on 9 March. The strong increase in Pdyn with arrival of the shock produced a Storm Sudden Commencement signature in SymH and inward motion of the Shue magnetopause (second panel). The AE index is also provided (third panel), correlated with increases in GOES 13 P1 flux, which has an effective energy of 2 MeV at this time (see Appendix **Figure A1** spectrum). This suggests that P1 is sensitive to substorm injections as well as increased SEP flux.

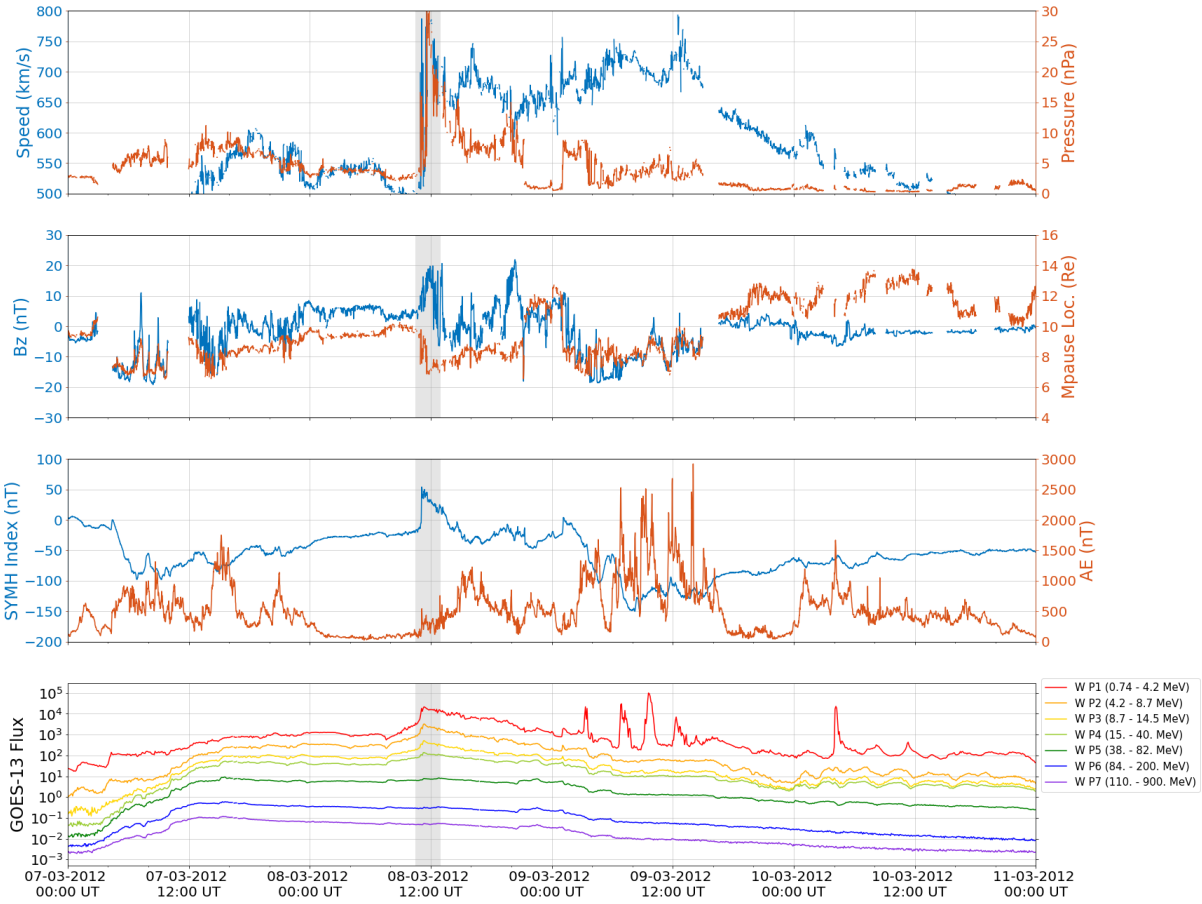

Figure 2. (Top 3 panels) Solar wind parameters, geomagnetic indices and magnetopause location calculated using the Shue et al. (1998) model from OMNIWeb for 7 – 11 March 2012. (Bottom)

SEP flux measured by the west-facing EPS instrument on GOES-13 (Grub, 1975). Gray shading indicates the time interval of the MHD-test particle simulation described below.

The Lyon-Fedder-Mobarry (LFM) MHD model combined with the Rice Convection Model (Lyon et al., 2004; Wiltberger et al., 2017) is used to calculate electric and magnetic fields for subsequent test particle simulation of the SEP response to arrival of the CME-shock. The LFM MHD model uses 1-minute solar wind parameters measured near the L1 orbit available from OMNIWeb, see Figure 2, propagated to the upstream boundary of LFM at x = 30 Re. The inner boundary of LFM is set to be 2 Re and IGRF fields are used in the region inside the LFM inner boundary in this study. The Rice Convection Model (RCM) is coupled to the LFM model to include ring current drift physics not present in ideal MHD (Pembroke et al., 2012; Wiltberger et al., 2017). The LFM model uses a computational domain extending from +30 Re to -300 Re along the sun-earth line (SM-x) and from -150 Re to +150 Re along SM-y and SM-z. All MHD input variables are assumed to be uniform in y and z at the upstream boundary. The LFM grid resolution is 106 x 96 x 128 along radial, azimuthal and polar directions. Coupling to the ionosphere uses an electrostatic potential solver incorporating changes in field-aligned currents and dynamic conductivities (Merkin and Lyon, 2010). The 3D MHD fields are dumped at 15s cadence for implementation in the test particle simulations.

The rbelt3d test particle code, which resolves 3D Lorentz trajectories (Kress et al., 2007), advances proton trajectories which can be traced as test particles in the MHD electric and magnetic fields. Test particle protons (4.9M in a flat spectrum from 0.1 – 5 MeV) are injected isotropically from a sphere at 7 Re to simulate the isotropic distribution of the solar wind SEPs which populate the magnetosphere into ~ 4 Re prior to and following arrival of the interplanetary shock seen in Figure 2. The access of SEPs into L = 3-4 has been seen in other data sets prior to Van Allen Probes such as CRESS (Hudson et al., 1997), SAMPEX (Kress et al., 2004) and HEO (Selesnick et al., 2010) measurements. Lorentz trajectories are followed for 150 minutes beginning at 1030 UT on 8 March with injection stopping at 1200 UT to distinguish the trapped proton radial profile by the end of the simulation at 1300 UT.

Sample proton test particles transported in the LFM-RCM fields for the March 2012 event are plotted in **Figure 3** in four equatorial plane projections around the time of the shock arrival. Results are consistent with acceleration and inward radial transport of protons in drift resonance with the azimuthal electric field impulse due to CME-shock compression of the dayside magnetopause (Li et al., 1993; Hudson et al., 1995; 1997). Similar drift resonant acceleration of outer zone electrons with CME-shock compression of the magnetopause has been seen for other events both in simulations and measurements going back to the 24 March 1991 CRRES observations of both proton and electron transport and fields (Blake et al., 1992; Wygant et al, 1994; see Hudson et al., 2020 for a review, and their Figure 6 for simulated $E_\varphi < 0$ impulse propagation around dawn and dusk flanks for the 17 March 2015 ‘St. Patrick’s Day storm’; also Kress et al., 2007 for the 2003 ‘Halloween storm’).

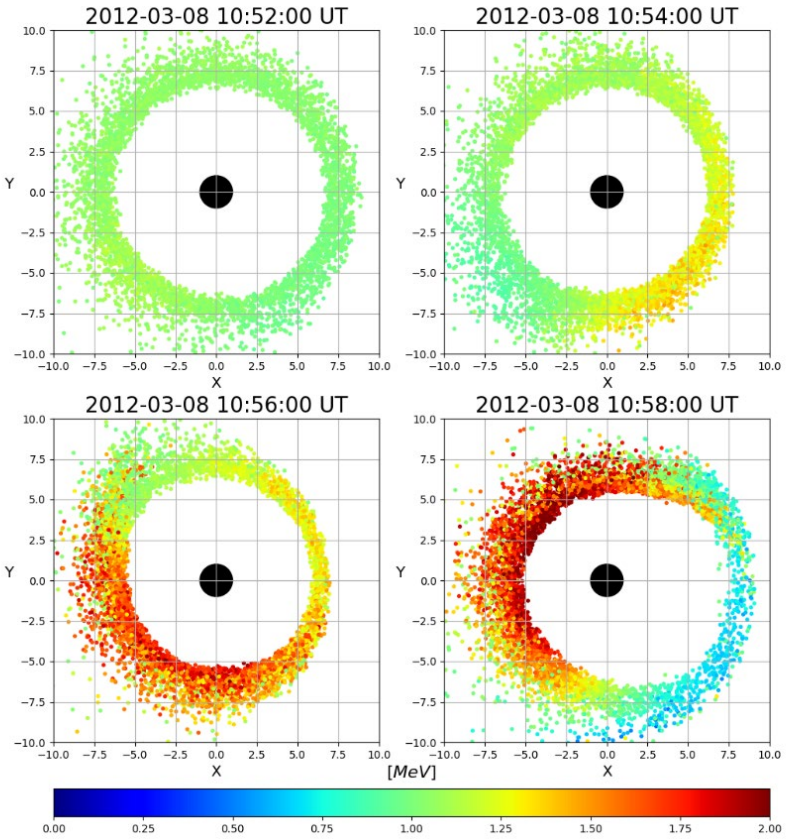

Figure 3. Equatorial plane snapshots of test particle protons with initial sample energy of 1 MeV injected into in LFM-RCM simulation fields driven by L1 solar wind parameters from OMNIWeb for the 8 March 2012 SEP trapping event, with energy of test particles at time plotted indicated in the color scale. Protons are injected isotropically from a sphere at 7 Re into the MHD fields, and are accelerated (red) by a negative (westward) azimuthal electric field due to the magnetopause compression as they drift from noon along the dawn side of the magnetosphere, while protons by 10:58 UT on the dayside interact with the positive (eastward) component of the bipolar electric field impulse characteristic of this type of dayside compression (Hudson et al., 2017; 2020) and are decelerated (blue). Perpendicular energy increase due to the azimuthal electric field maximum in the equatorial plane (Kress et al., 2007) results in trapping. View plotted is projection onto the equatorial plane of all injected protons which are seen to be completing a drift orbit over the times shown.

Figure 4 shows Phase Space Density (PSD) vs. L and time at 1000 MeV/G from the MHD-test particle simulation for 8 March 2012, corresponding to 1 MeV at geosynchronous and 37.5 MeV at L = 2 in a dipole. Protons are initially filtered by equatorial pitch angles between 85 - 95 degrees, a bin width optimized for counting statistics around 90 degrees, since the subsequent radial diffusion calculation is a function of L only at fixed first invariant (Li et al., 2017). Particle weights are calculated using Equation 10 from Kress et al (2008) where flux is provided from GOES-13 and GOES 15 measurements by the Energetic Particle Sensor instrument (Grub, 1975). A sample spectrum during the SEP event at 0 UT on 8 March 2012 is shown in the

Appendix **Figure A1**, where the effective energy of the P1 (lowest energy) detector is approximately 2 MeV. Following the SEP event, the effective energy of the P1 detector drops to 1 MeV as described further in the Appendix. Flux measurement at geosynchronous is used to weight the injected test particles and the injection is stopped at 12 UT in order to subsequently distinguish trapped protons from the SEP source. Conversion from spherical coordinates in the SM equatorial plane of LFM-RCM to McIlwain L was performed using the IRBEM library which converts LFM-RCM fields from SM-r to McIlwain L (https://sourceforge.net/p/irbem/wiki/Home/), using 5 min averaged time-varying solar wind parameters taken from OMNIWeb. This was found to affect only higher L values, not L = 3-4 where trapping occurs. Therefore results are shown in dipole L. Particles are assigned the appropriate initial weights and binned by energy (0.25 MeV), L (0.2 Re) and time (5s). The simulated flux is then given by Equation 8 from Kress et al (2008) where the flux is a function of L and time.

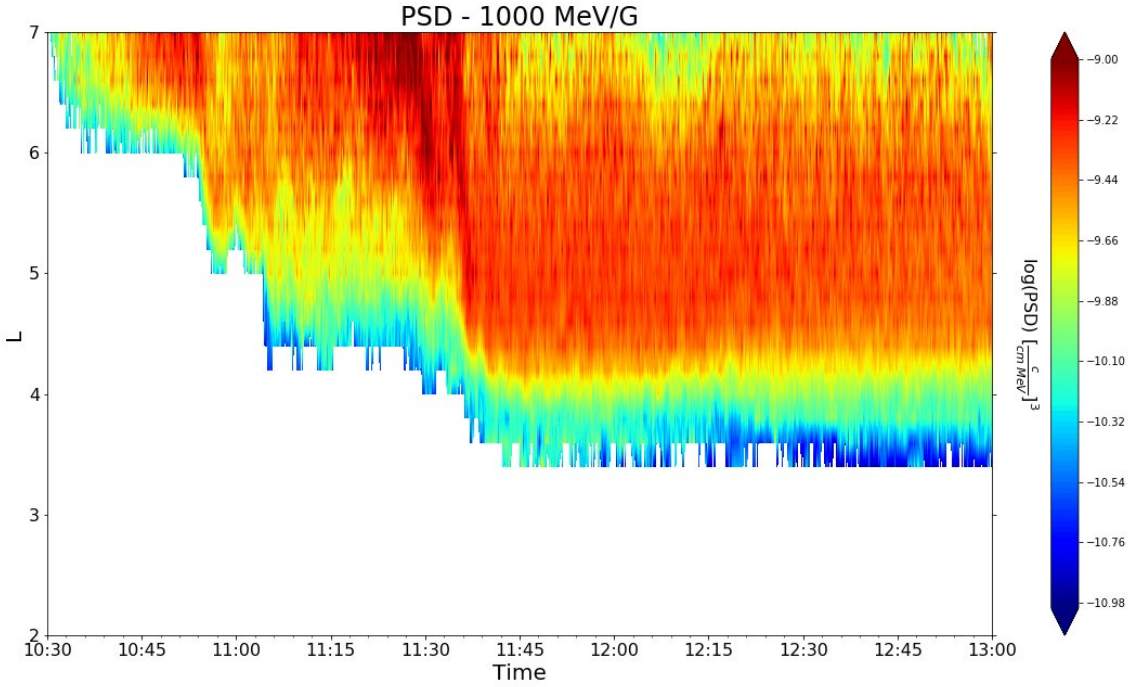

Figure 4. 1000 MeV/G electron log Phase Space Density in the equatorial plane calculated from MHD-test particle simulations for the 8 March 2012 SEP trapping event in the units of $(c/MeV/cm)^3$. Results are shown in dipole L. The last 10 minutes of the simulated PSD is time-averaged to provide the initial radial profile for the subsequent radial diffusion calculation.

Phase Space Density f can be calculated from flux j as $f = j/p^2$ for 90-degree equatorial pitch angles, where p is the relativistic momentum. The simulation data is further filtered by a constant first adiabatic invariant value ± 250 MeV/G. The final data product from the MHD-test particle simulations is f as a function of L and time for a given first invariant. Additional first invariants have been simulated (1500 and 2000 MeV/G) corresponding to 56 and 75 MeV at L = 2, see **Figure A2**.

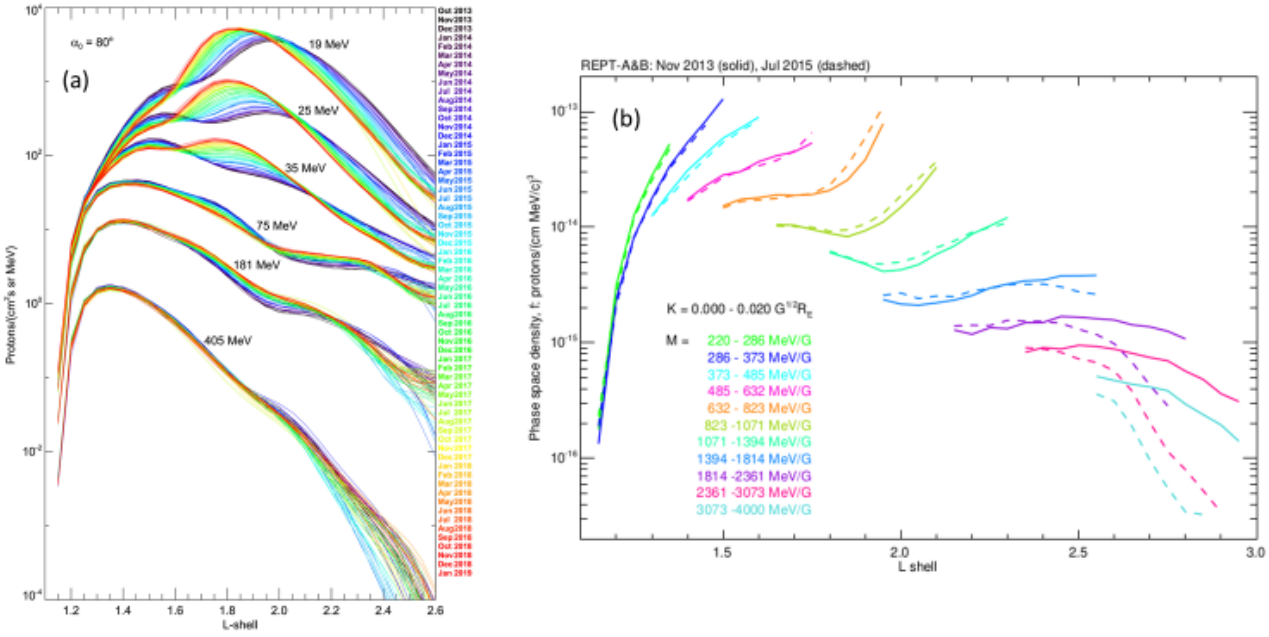

hh

Figure 5. a) Proton intensity versus L as measured by the REPT instrument on Van Allen Probes at selected energies, with equatorial pitch angle α_0=80°, for consecutive color-coded monthly averages (Selesnick and Albert, 2019). Figure has been updated through the end of the Van Allen Probes mission in 2019, see Baker et al., 2021, Figure 50. **b)** Phase space density versus L for the indicated fixed ranges of the first and second adiabatic invariants, M and K, measured by REPT-A and REPT-B. Monthly averages are included from November 2013 (solid curves) and July 2015 (dashed curves). K range corresponds to near-equatorially mirroring protons (Selesnick et al., 2016).

4. 8 March 2012 SEP trapping event: radial diffusion calculation

In order to compare the MHD-test particle simulation of the 8 March 2012 trapping event with the inner zone protons *following* the launch of Van Allen Probes (August 30, 2012), a radial diffusion calculation has been implemented with input from the simulated trapping event using a radial diffusion code developed by Li et al. (2017) and the diffusion coefficient implemented by Selesnick and Albert (2019), $D_{LL} = D_0 L^{10} y^{1.6}$, shown to reproduce the evolution of the inner zone proton flux profile seen in Figure 5a. In fitting a radial diffusion model to the data plotted, Selesnick and Albert (2019) found D_0=7×10^{-14} s^{-1} before 1 January 2015, where y=1 for the sine of equatorial pitch angle in our equatorial plane implementation. No first invariant (or energy) dependence was required. After 1 January 2015 D_0 was found to be larger by a factor of 2 (Selesnick and Albert, 2019), so this can be taken as a range of uncertainty in D_0 used for the radial diffusion calculation covering two years beginning 8 March 2012. An initial radial profile

for the diffusion calculation at fixed first invariant is obtained by weighting test particle protons as described above using GOES measurements and converting from flux to phase space density. The GOES data set used to weight phase space density f in Figure 4 is also used to provide the outer boundary condition at 6.6 Re for subsequent radial diffusion over the time interval studied, in practice using the flux from the lowest energy channel of EPS which is nominally ~1 MeV during non-SEP intervals (see Appendix). So that only trapped protons are included, the initial radial profile for the radial diffusion calculation is taken from averaging over the last 10 minutes of the phase space density profile in Figure 4, computed from flux-weighted test particles using their final energy and the local MHD magnetic field to compute a fixed first invariant.

Figure 6 shows Phase Space Density at 1000 MeV/G evolved over two years following the trapping event simulated in Figure 4. The effect of subsequent increases in PSD at the GOES outer boundary are seen due to weaker SEP events (21 during the two year interval studied, see ftp://ftp.swpc.noaa.gov/pub/indices/SPE.txt for events with > 10 MeV protons exceeding a flux of $10/cm^{-2}$-s-sr), and increases in flux at 1 MeV due to substorm injections as seen in Figure 2. The effect of both subsequent weaker SEP events and substorm injections is investigated by setting the outer boundary to zero (blue dashed curve) in the right panel of Figure 6. This curve falls on top of that obtained including the GOES measured flux at 1 MeV for the outer boundary condition (yellow). A second experiment was performed including only the GOES outer boundary condition and removing the initial radial profile from the MHD-test particle simulation obtained from Figure 4 (red), demonstrating that the initial strong SEP event dominated the PSD enhancement at L = 2. The PSD on Day 616 (15 Nov 2013) at L = 2 following the 8 March 2012 (Day 0) injection was 3.7×10^{-14} (same units as Figure 4) as compared with that measured by REPT at 1000 MeV/G, the light green curve (823 – 1071 MeV/G) in Figure 5b, which was 1×10^{-14} at L =2. Similar results to Figure 6b are plotted at other first invariants corresponding to 56 MeV (1500 MeV/G) and 75 MeV (2000 MeV/G) at L = 2, see Appendix **Figure A3**. At 1500 MeV/G the simulated PSD on 15 Nov 2013 is 1×10^{-14} and measured (1394 – 1814 MeV/G) in Figure 5b is 2×10^{-15} at L = 2. The SEP contribution is relatively greater at lower L for the lower first invariant and superimposed on the CRAND contribution which is greater at higher L for the higher first invariant.

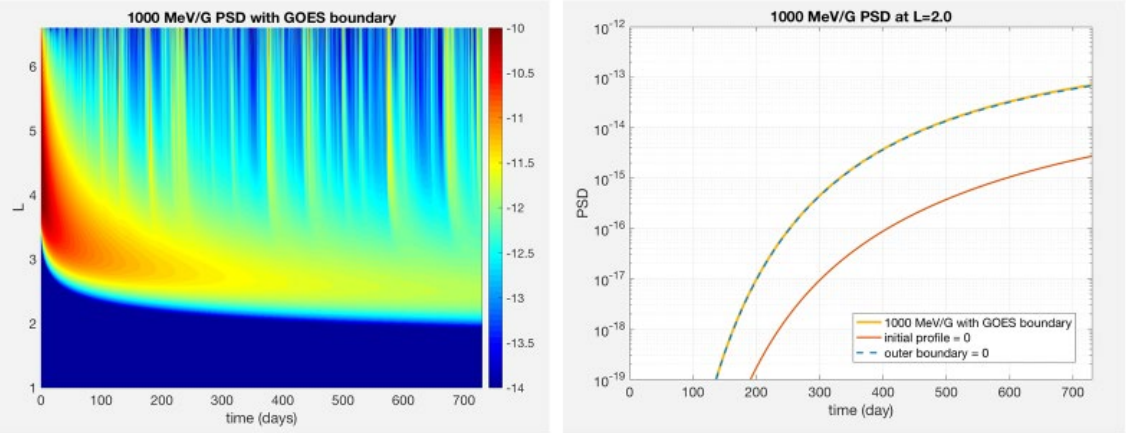

Figure 6. (Left) Simulated Phase Space Density (PSD log color scale in same units as Figure 4) vs. L and time produced with a radial diffusion code (Li et al., 2017) and D_{LL} consistent with the range of D_0 (7 x 10^{-14} s^{-1}) found by Selesnick and Albert (2019) to reproduce REPT measurements in Figure 5a. The radial diffusion result is shown over two years following the 8 March 2012 SEP trapping event simulated in Figure 4 using the MHD-test particle code. Diffusion in L is initialized with a radial profile averaged over the last 10 minutes of Figure 4 and updated hourly with GOES 13 measurements at 1 MeV converted to PSD at the outer boundary, shown for 1000 MeV/G which corresponds to 37.5 MeV at L = 2. (Right) PSD vs. time at L = 2 (yellow) and for comparison, radial diffusion result with the outer boundary set to zero after t= 0 (blue dashed curve) and with the initial radial profile set to zero (red) maintaining the GOES outer boundary, to examine the relative importance of the initial SEP injection and variations at GOES due to subsequent SEP events and substorm injections modulating the 1000 MeV/G PSD (~ 1 MeV flux) at L = 6.6.

5. Discussion and Conclusions

While earlier work using data from HEO spacecraft (Selesnick et al., 2010) provided insight into the SEP flux level and geomagnetic conditions that lead to trapping, it lacked pitch angle resolution and the energy resolution of the Van Allen Probes REPT data set, which was in a near equatorial, geosynchronous transfer orbit capturing the peak of the trapped proton flux at 90 degrees. A persistent feature of the inner zone proton flux vs. L during the entire 7 years of the Van Allen Probes mission is the double peaked inner zone at lower REPT energies evident in Figure 5a. Selesnick et al. (2016) suggested that an earlier SEP event prior to the launch of Van Allen Probes could be responsible for this lower energy-higher L component of the inner zone, consistent with earlier modeling of long-term inner zone dynamics.

The trapping event simulated in Figure 3 for 8 March 2012, the strongest SEP event of Solar Cycle 24, occurs on the timescale of the proton drift. A bipolar azimuthal electric field was first measured in situ simultaneously with an increase in the compressional component of the magnetic field by the CRRES satellite for the March 1991 proton and electron injection event

(Wygant et al., 1994), and again for other CME-shock compressions of the dayside magnetopause, consistent with Faraday's Law (see review by Hudson et al., 2020). This perturbation propagates at the MHD fast mode or magnetosonic speed around the dawn and dusk inner flanks of the magnetopause and has been observed by multiple spacecraft and seen in ground magnetometer measurements simultaneously with Van Allen Probes electric and magnetic field measurements (see for example Paral et al., 2015, Figure 4 and discussion). As first noted by Li et al. (1993), applied to electrons and subsequently to protons (Hudson et al., 1995; 1997), the azimuthal electric field impulse points in a direction (westward) favorable to both proton acceleration along the dawn flank and electron acceleration along the dusk flank. SEPs populate the magnetosphere into L ~ 4 prior to arrival of the interplanetary shock since SEPs typically travel at higher speeds than the shock (Reams et al., 2001). The acceleration seen in Figure 3 increases proton perpendicular energy due to E_φ, resulting in a change in pitch angle towards 90 degrees. Inward radial transport and trapping follows from conservation of the first adiabatic invariant. As previously noted (Hudson et al., 1995; 1997), protons in drift resonance on the dawn side (like electrons on the dusk side) drifting azimuthally at approximately the magnetosonic speed (~ 800 - 1000 km/s is a typical fast mode speed around geosynchronous, Paral et al., 2015) see an approximately constant electric field in their frame of reference. This produces a velocity filter effect, a proton energy range with azimuthal drifts comparable to the E_φ impulse (Hudson et al., 1996). **Figure 7** plots proton drift velocity vs. energy at different L values for a dipole magnetic field. A 1 MeV proton drifts azimuthally at 800 km/s at L = 7, the outer boundary of the MHD-test particle injection simulation. Protons up to 5 MeV also have direct access into L = 3-4, where they can interact resonantly with E_φ (have comparable azimuthal velocity) increasing their equatorial pitch angle to become trapped. Thus protons in the energy range simulated (0.1 – 5 MeV) which are injected isotropically from a sphere at 7 Re can be become trapped, as seen in Figure 4. MHD-test particle experiments with higher energy proton injection, for example > 20 MeV, did not show trapping.

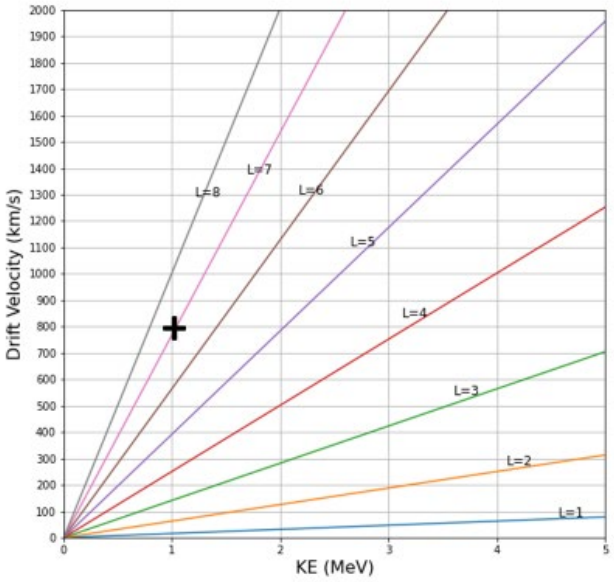

Figure 7. Plot of proton drift velocity vs. energy at different L values for a dipole magnetic field. A 1 MeV proton drifts at 800 km/s azimuthally at L = 7, indicted by the cross, at the outer boundary of the injection simulation. Thus protons in this energy range (0.1 – 5 MeV were injected) can be perpendicularly accelerated and trapped as seen in Figure 4.

In order to compare results with REPT proton measurements available as Phase Space Density beginning October 2013 (Figure 5b, Selesnick et al., 2016), results from the MHD-test particle simulation of the trapping were provided as input to a radial diffusion calculation over the subsequent two years using the radial diffusion code developed by Li et al. (2017) and diffusion coefficient from Selesnick and Albert (2019). An initial radial profile from the MHD-test particle simulations weighted by measured GOES flux at geosynchronous was used to initialize the radial diffusion calculation, and hourly GOES measurements were used to update the outer boundary for the 1000 MeV/G case. It was found that the simulation was not sensitive to subsequent smaller SEP events and substorm injections, consistent with Selesnick et al. (2007, Figure 15), which presented inner zone model results over 35 years (1970 – 2005), showing strong SEP events dominating the proton flux near 90 degree pitch angles at lower energies and higher L values. The CRAND process dominates higher energies and lower L values. Similar results were obtained in our radial diffusion study at two higher first invariants, 1500 and 2000 MeV/G. The outer boundary was set to zero for the two higher invariants based on insensitivity of the results to small variations in the outer boundary in the 1000 MeV/G case (Figure 6b). A comparison of phase space density evolution at the three invariants is shown in **Figure A3**.

A direct comparison with REPT measurements in November 2013 following the trapping event in March 2012 provides a test of this combination of short-term and long-term evolution of the newly trapped protons. The simulation results were found to produce reasonable agreement with measured PSD, given that no losses were included in the model, such as magnetic field line curvature scattering due to geomagnetic storms (Engel et al., 2016), of which there were eight with Dst $\leq$ -100 nT between 8 March 2012 and 15 November 2013. Loss due to atmospheric scattering is negligible at L $\geq$ 2 at the energies studied (Selesnick et al., 2007). Including losses in the model could lower the simulated PSD relative to measured, 3.7 x 10^{-14} vs. 1 x 10^{-14}, respectively, for 1000 MeV/G at L = 2.

The L-dependence of trapping can also be investigated by comparing the inner boundary of the PSD from the MHD-test particle simulations for the first invariants studied. **Figure A2** shows that lower energy protons are transported and trapped at lower L than higher energy protons, comparing the 1000, 1500 and 2000 MeV/G cases. This result might seem counterintuitive relative to cutoffs which occur at lower L at higher energies (Li et al., 2021 and references). However, the latter well known dependence applies to untrapped protons. Instead, Figure 7 shows that lower energy protons ~ 1 MeV (1000 MeV/G at geosynchronous) are more favorably in drift resonance with a magnetosonic impulse travelling azimuthally at 800 km/s than higher energy protons, with greater inward radial transport conserving the first invariant. This fast mode propagation speed around geosynchronous orbit which scales as $B/\sqrt{\rho}$ in terms of unperturbed magnetic field and cold plasma density is relatively invariant at the beginning of CME-shock events, changing on a longer time scale than the impulse propagation speed of a few minutes through the magnetosphere (Araki et al., 1997).

In summary, the MHD-test particle simulations demonstrate the causal role that the inductive electric field played in trapping protons for the March 2012 SEP event. The simulations also support the hypothesis by Selesnick et al. (2016) that a strong SEP event prior to the launch of Van Allen Probes was responsible for the higher L, lower energy peak of the inner zone evident during the 7 years of the mission. This type of inner zone structure is not always seen and it appears to take a particularly strong SEP event to produce in terms of proton flux (Selesnick et al., 2010). While there were no comparable events during the lifetime of the Van Allen Probes mission from 30 August 2012 to 18 October 2019 (ftp://ftp.swpc.noaa.gov/pub/indices/SPE.txt), a quiet solar cycle by all measures (Bregou et al., 2021), more frequent SEP trapping events are evident in the model calculation of Selesnick et al. (2007, Figure 15) from 1970 - 2005 during more active solar cycles. The two timescale simulation results presented here confirm that SEP trapping can explain the two-component structure of the inner zone seen throughout the lifetime of the Van Allen Probes mission along with the CRAND source at higher energies and lower L (Selesnick et al., 2016), and should be included in any long-term inner zone model.

Appendix

The following figures supplement the main text. **Figure A1** shows a sample spectrum from GOES 13 and 15 of the flux used to weight the MHD-test particle simulations. Subsequent spectra were provided at 1-hour intervals over two years following this time as an outer boundary condition for the radial diffusion calculation. **Figure A2**, same format as Figure 4, compares PSD from the MHD-test particle simulations at three first invariants. **Figure A3** plots the PSD vs. time from the radial diffusion calculation for these three first invariants (1000, 1500 and 2000 MeV/G) using the initial radial profile from the MHD-test particle simulations with the outer boundary set equal to zero, since Figure 6b shows that the outer boundary has relatively little impact on the final result compared to the initial SEP event.

Figure A1 shows a sample spectrum from GOES 13 and 15 Energetic Particle Sensors (EPSs) [Grub, 1975] of the flux used to weight the MHD-test particle simulations. Since the GOES EPS energy channels are very broad (e.g., EPS P1 FWHM energy bounds are 0.74-4.2 MeV), the spectra are obtained using an iterative fitting method as described in Section 5 of Kress et al. [2021], which also returns a channel effective energy. Spectra were obtained at 1-hour intervals to weight test-particles injected into the LFM-RCM fields throughout the MHD-test particle simulation. The test-particles are weighted using Equation 10 from Kress et al. [2008]. Spectra from the GOES-13 west viewing unit is used since it most closely represents the interplanetary spectrum.

During the 8 March 2012 SEP event, the EPS P1 effective energy is 1.8-1.9 MeV. During quiet solar conditions when there is no solar particle event, magnetospheric proton fluxes fall off very rapidly at geosynchronous with energy above 1 MeV, and the GOES EPS P2 channel is at background level. To obtain an outer boundary condition for the subsequent radial diffusion calculation, the GOES EPS measurements were augmented with 80-800 keV measurements from the GOES Magnetospheric Proton Detector (MAGPD) [Rodriguez et al., 2020]. Assuming zero proton flux above the P1 channel midpoint energy (~2.5 MeV), we find that the P1 effective energy is approximately 1 MeV during quiet solar periods. EPS P1 flux at a 1-hour cadence, over two years following the March 2012 SEP event, were used as an outer boundary condition for the radial diffusion calculation, taking 1 MeV as the effective energy for the P1 channel.

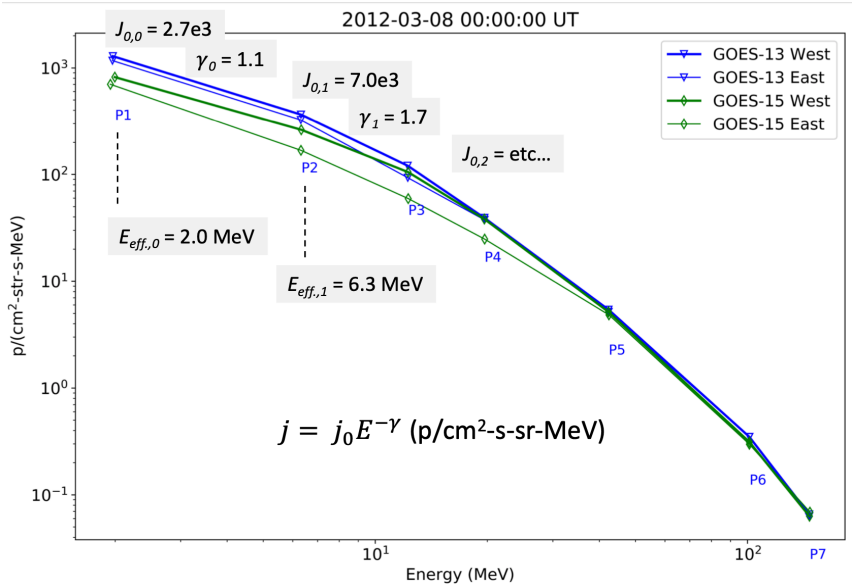

A1. An initial energy spectrum of injected test particles into MHD fields for conversion to flux by the method described in Kress et al. (2008) and for the radial diffusion calculation outer boundary at L = 6.6 can be provided by the GOES 13 and GOES 15 Energetic Particle Sensor measurements, providing a spectrum which can be extrapolated to lower (and higher) energies as needed to cover the first invariant range studied (500, 1000, and 2000 and 4000 MeV/G). P1 through P7 indicate different energy channels of the EPS instrument on GOES (Grub, 1975) and different j_0 and γ indexed by linear fit of the j power law function to each energy channel. Note that west is lower than east-facing detector flux due to the finite proton gyroradius at these energies, so lower energy protons gyrate from higher L and higher from lower L into west and east facing detectors respectively, with flux higher at lower energies.

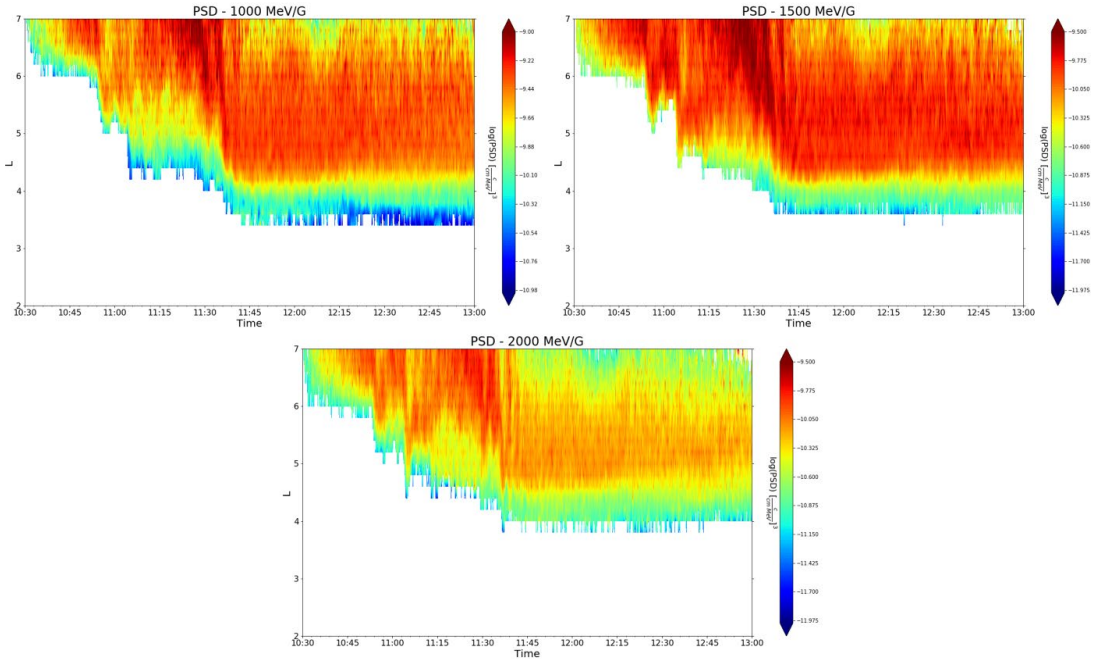

Figure A2. Phase Space Density vs. L and time from MHD-test particle simulations at 1000, 1500 and 2000 MeV/G. All parameters are the same as Figure 4 for simulation of the 8 March 2012 SEP trapping event PSD over the time interval of the vertical gray stripe in Figure 2, The inner boundary of the trapped population is L ~3.5 at 1000 MeV/G and L=4 at 2000 MeV/G and between those values at 1500 MeV/G.

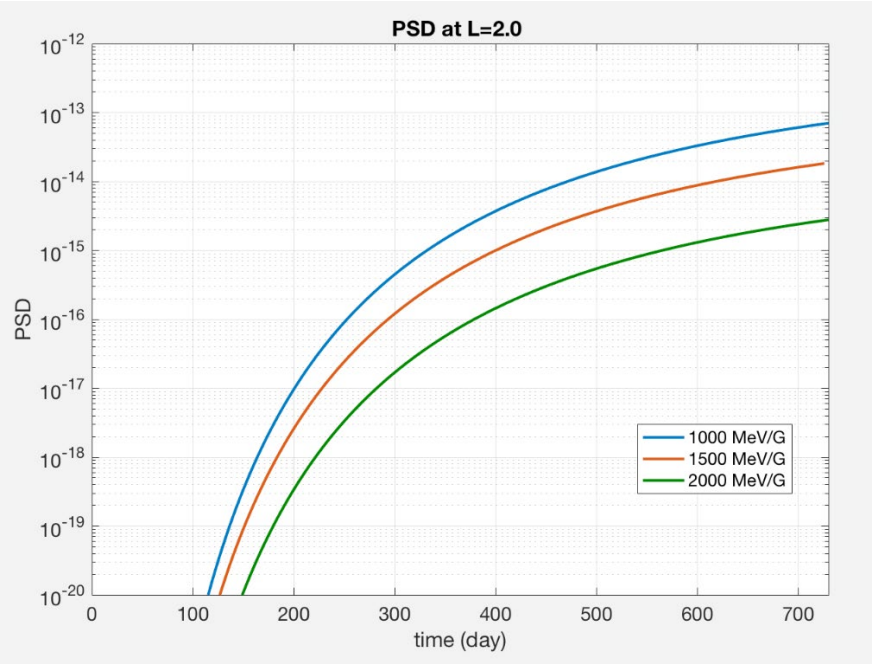

Figure A3. Comparison of radial diffusion results in Figure 6b at three first invariants, all without the outer boundary update which Figure 6b shows has a small impact on the result relative to the initial radial profile from the MHD-test particle simulations.

Acknowledgments

Dartmouth College and University of Colorado acknowledge support from AFOSR grant FA9550-20-1-0339. The authors acknowledge high-performance computing support from NCAR CISL.

Data Availability Statement

Solar wind data can be accessed at https://omniweb.gsfc.nasa.gov. Van Allen Probe REPT/ECT data can be accessed at the website (https://www.rbsp-ect.lanl) and NOAA GOES 13 and 15 data at https://satdat.ngdc.noaa.gov/sem/goes/data/. The simulation data output is available via the Zenodo website (https://doi.org/10.5281/zenodo.7236154).

References

Araki, T., et al. (1997), Anomalous sudden commencement on March 24, 1991, *J. Geophys. Res.*, 102(A7), 14075– 14086, doi:10.1029/96JA03637.

Baker, D. N., et al. (2012), The Relativistic Electron-ProtonTelescope (REPT) instrument on board the Radiation Belt Storm Probes (RBSP) spacecraft: characterization of Earths radiation belt high-energy particle populations, *Space Sci. Rev.*, doi:10.1007/s11214-012-9950-9.

Baker, D.N., Kanekal, S.G., Hoxie, V. et al., (2021), The Relativistic Electron-Proton Telescope (REPT) Investigation: Design, Operational Properties, and Science Highlights. *Space Sci Rev* **217,** 68, doi: 10.1007/s11214-021-00838-3

Blake, J. B., W. A. Kolasinski, R. W. Fillius, E. G. Mullen, (1992) Injection of electrons and protons with energies of tens of MeV into L < 3 on March 24, 1991, *Geophys. Res. Lett., 19, 821.*

Blake, J., Carranza, P. A., Claudepierre, S. G., Clemmons, J. H., Crain, W. R., Dotan, Y., et al. (2013). The Magnetic Electron Ion Spectrometer (MagEIS) instruments aboard the Radiation Belt Storm Probes (RBSP) spacecraft. *Space Science Reviews*, *179*. https://doi.org/10.1007/s11214-013-9991-8

Engel, M. A., B. T. Kress, M. K. Hudson, and R. S. Selesnick (2016), Comparison of Van Allen Probes radiation belt proton data with test particle simulation for the 17 March 2015 storm, *J. Geophys. Res. Space Physics,* 121, 11,035–11,041, doi:10.1002/2016JA023333.

Filwett, R. J., Jaynes, A. N., Baker, D. N., Kanekal, S. G., Kress, B., & Blake, J. B. (2020). Solar energetic proton access to the near‐equatorial inner magnetosphere. *Journal of Geophysical Research: Space Physics*, 125, e2019JA027584. https://doi.org/ 10.1029/2019JA027584.

Grub, R. N. (1975). The SMS/GOES space environment monitor subsystem. NOAA technical Memorandum ERL SEL-42. Boulder, CO: Space Environment Laboratory.

Gussenhoven, M. S., E. G. Mullen, and D. H. Brautigam (1996), Improved understanding of the Earth's radiation belts from the CRRES satellite, *IEEE Trans. Nucl. Sci.*, 43(2):353–368.

Hudson, M.K., et al., (1995). Simulation of proton radiation belt formation during the March 24, 1991 SSC. Geophys. Res. Lett. https://doi.org/10.1029/95GL00009

Hudson, M. K., S.R. Elkington, J.G. Lyon, V.A. Marchenko and I. Roth (1996), MHD/particle simulations of radiation belt formation during a storm sudden commencement, AGU Geophysical Monograph 97, Radiation Belts: Models and Standards, pp. 57-62, 1996.

Hudson, M. K., S. R. Elkington, J. G. Lyon, V. A. Marchenko, I. Roth, M. Temerin, J. B. Blake, M. S. Gussenhoven, J. R. Wygant (1997), Simulations of radiation belt formation during storm sudden commencements, *J. Geophys. Res., 102(A7)*, 14,087–14,102, doi:10.1029/97JA03995.

Hudson, M., B. Kress, J. Mazur, K. Perry, *and* P. Slocum *(*2004*),* 3D modeling of shock-induced trapping of solar energetic particles in the Earth's magnetosphere*, J. Atmos. Sol. Terr. Phys.*, *66(15–16),* 1389–1397*,* doi:10.1016/j.jastp.2004.03.024.

Hudson M.K., A.N Jaynes, B.T. Kress, Z. Li, M. Patel, X.-C. Shen, S.A. Thaller, M. Wiltberger, *and* J. Wygant *(*2017*),* Simulated prompt acceleration of multi-MeV electrons by the 17 March 2015 interplanetary shock*, J. Geophys. Res.*, 122*,* doi:10.1002/2017JA024445.

Hudson, M. K., S. R. Elkington, Z. Li, and M. Patel (2020), Drift echoes and flux oscillations: A signature of prompt and diffusive changes in the radiation belts, *Journal of Atmospheric and Solar-Terrestrial Physics*, 207, doi:10.1016/j.jastp.2020.105332.

Hudson, M.K. et al. (2021), Simulated Trapping of Solar Energetic Protons as Measured by Van Allen Probes for the 7-8 September 2017 Geomagnetic Storm, AGU Fall Meeting.

King, J. H. and Papitashvili, N. E. (2005), Solar wind spatial scales in and comparisons of hourly wind and ace plasma and magnetic field data, *J. Geophys. Res.*, 110 (A2). doi: 10.1029/2004ja010649.

Kress, B. T., M.K. Hudson, K.L. Perry and P.L. Slocum (2004), Dynamic modelling of geomagnetic cutoff for the November 23 - 24, 2001 solar energetic particle event, *Geophys. Res. Lett*., 31, p. L04808.

Kress, B. T., Hudson, M. K., Slocum, P. L. (2005), Impulsive solar energetic ion trapping in the magnetosphere during geomagnetic storms, *Geophys. Res. Lett*., Vol. 32, No. 6, L06108.

Kress, B. T., M. K. Hudson, M. D. Looper, J Albert, J. G. Lyon, and C. C. Goodrich (2007), Global MHD test particle simulations of >10 MeV radiation belt electrons during storm sudden commencement, *J. Geophys. Res., 112,* A09215, doi:10.1029/2006JA012218.

Kress, B. T., M. K. Hudson, M. D. Looper, J. G. Lyon, and C. C. Goodrich (2008), Global MHD Test Particle Simulations of Solar Energetic Electron Trapping in the Earth's Radiation Belts, J. of Atmospheric & Solar-Terrestrial Physics, Vol 70/5, 10.1016/j.jastp.200711.003, 2008.

Kress, B. T., C. J. Mertens, and M. Wiltberger (2010), Solar energetic particle cutoff variations during the 29-31 October 2003 geomagnetic storm, *Space Weather, 8*, S05001, doi:10.1029/2009SW000488.

Kress, B.T., J.V. Rodriguez, J.E. Mazur, M. Engel (2013), Modeling solar proton access to geostationary spacecraft with geomagnetic cutoffs, Adv. Space Res., 52, 11, pg. 1939-1948, doi: 10.1016/j.asr.2013.08.019.

Kress, B. T., M. K. Hudson, R. S. Selesnick, C. J. Mertens, and M. Engel (2015), Modelling geomagnetic cutoffs for space weather applications, *J. Geophys. Res. Space Physics*, 120, 5694–5702, doi: 10.1002/2014JA020899.

Kress, B. T., Rodriguez, J. V., Boudouridis, A., Onsager, T. G., Dichter, B. K., Galica, G. E., & Tsui, S. (2021). Observations from NOAA's newest solar proton sensor. *Space Weather*, *19*, e2021SW002750. https://doi. org/10.1029/2021SW002750

Li, Z., M. K. Hudson, M. Patel, M. Wiltberger, A. Boyd, and D. Turner (2017), ULF wave analysis and radial diffusion calculation using a global MHD model for the 17 March 2013 and 2015 storms, J. Geophys. Res. Space Physics, 122, *doi:*10.1002/2016JA023846.

Li, Z., Engel, M., Hudson, M., Kress, B., Patel, M., Qin, M., & Selesnick, R. (2021). Solar Energetic Proton Access to the Inner Magnetosphere during the 7-8 September 2017 event. *Journal of Geophysical Research: Space Physics*, 126, e2021JA029107. https://doi.org/10.1029/2021JA029107

Looper, M. D., J. B. Blake, and R. A. Mewaldt (1998), Maps of Hydrogen isotopes at low altitudes in the inner zone from SAMPEX observations, *Adv. Space. Res., 21*, 12,1679–1682.

Lyon, J., J. Fedder, *and* C. Mobarry (2004), The Lyon-Fedder-Mobarry (LFM) global mhd magnetospheric simulation code, *J. Atmos. Sol. Terr. Phys.*, *66(*15–16*),* 1333–1350, doi:10.1016/j.jastp.2004.03.020.

Mauk, B. H., N. J. Fox, S. G. Kanekal, R. L. Kessel, D. G. Sibeck, A. Ukhorskiy (2012), Science objectives and rationale for the Radiation Belt Storm Probes mission, *Space Sci. Rev.*, doi:10.1007/s11214-012-9908-y.

Mazur, J. E., Blake, J. B., Slocum, P. L., Hudson, M. K. and Mason, G. M. (2006) The Creation of New Ion Radiation Belts Associated with Solar Energetic Particle Events and Interplanetary Shocks, in Solar Eruptions and Energetic Particles (eds N. Gopalswamy, R. Mewaldt and J. Torsti), American Geophysical Union, Washington, D. C.. doi: 10.1029/165GM32.

Mazur, J. et al. (2013), The Relativistic Proton Spectrometer (RPS) for the Radiation Belt Storm Probes Mission, *Space Science Reviews,* 179:221–261, doi:10.1007/s11214-012-9926-9.

Mitchell, D.G., Lanzerotti, L.J., Kim, C.K. *et al.* Radiation Belt Storm Probes Ion Composition Experiment (RBSPICE). *Space Sci Rev* **179,** 263–308 (2013). https://doi.org/10.1007/s11214-013-9965-x

O'Brien, T. P., Mazur, J. E., & Looper, M. D. (2018). Solar energetic proton access to the magnetosphere during the 10 - 14 September 2017 particle event, *Space Weather*, 16. https://doi.org/10.1029/2018SW001960.

Pembroke, A., F. Toffoletto, S. Sazykin, M. Wiltberger, J. Lyon, V. Merkin, and P. Schmitt (2012), Initial results from a dynamic coupled magnetosphere - ionosphere -ring current model, *J. Geophys. Res.*, 117, A02211, doi: 10.1029/2011JA016979.

667 Qin, M., Hudson, M., Kress, B., Selesnick, R., Engel, M., Li, Z., & Shen, X. (2019).
668 Investigation of Solar Proton Access into the inner magnetosphere on 11 September 2017.
669 *Journal of Geophysical Research: Space Physics*, 124. https://doi.org/10.1029/2018JA026380
670
671 Reames, D.V. (2001). Seps: Space Weather Hazard in Interplanetary Space. In Space Weather
672 (eds P. Song, H.J. Singer and G.L. Siscoe). https://doi.org/10.1029/GM125p0101
673
674 Rodriguez, J. V., Denton, M. H. & Henderson, M. G. (2020), On-orbit calibration of
675 geostationary electron and proton flux observations for augmentation of an existing empirical
676 radiation model, *J. Space Weather Space Clim., 10*, https://doi.org/10.1051/swsc/2020031.
677
678 Sawyer, D. M. and J. I. Vette (1976), *AP-8 trapped proton environment for solar maximum*
679 *and solar minimum*, technical report, NASA-TM-X-72605, NSSDC/WDC-A-R/S-76-
680 06.
681
682 Selesnick, R. S., M. D. Looper, and R. A. Mewaldt (2007), A theoretical model of the inner
683 proton radiation belt, *Space Weather, 5*, S04003, doi:10.1029/2006SW000275.
684
685 Selesnick, R. S., M. K. Hudson, and B. T. Kress (2010), Injection and loss of inner
686 radiation belt protons during solar proton events and magnetic storms, *J. Geophys. Res., 115*,
687 A08211, doi:10.1029/2010JA015247.
688
689 Selesnick, R. S., M. K. Hudson, and B. T. Kress (2013), Direct observation of the CRAND proton
690 radiation belt source, *J. Geophys. Res., 118*, doi:10.1002/2013JA019338.
691
692 Selesnick, R. S., D. N. Baker, A. N. Jaynes, X. Li, S. G. Kanekal, M. K. Hudson, and B. T. Kress
693 (2014), Observations of the inner radiation belt: CRAND and trapped solar protons, *J. Geophys.*
694 *Res.*, 119, 6541–6552, doi:10.1002/2014JA020188.
695
696 Selesnick, R. S., D. N. Baker, A. N. Jaynes, X. Li, S. G. Kanekal, M. K. Hudson, and B. T. Kress
697 (2016), Inward diffusion and loss of radiation belt protons,
698 *J. Geophys. Res.*, 121, 3, doi:10.1002/2015ja022154.
699
700 Selesnick, R. S., & Albert, J. M. (2019). Variability of the proton radiation belt. *Journal of*
701 *Geophysical Research: Space Physics*, 124, 5516– 5527. https://doi.org/10.1029/2019JA026754.
702
703 Smart, D. F. and M.A. Shea (2009), Fifty years of progress in geomagnetic cutoff rigidity
704 determinations, *J. Adv. Space Res., 44,* 1107–1123, doi:10.1016/j.asr.2009.07.005.
705
706 Vacaresse, A., D. Boscher, S. Bourdarie, M. Blanc, and J. A. Sauvaud (1999),
707 Modeling the high-energy proton belt, *J. Geophys. Res., 104*, 28,601–28,613,
708 doi:10.1029/1999JA900411.
709
710 Wiltberger, M., et al. (2017), Effects of electrojet turbulence on a magnetosphere ‐
711 ionosphere simulation of a geomagnetic storm, *J. Geophys. Res. Space Physics*, 122, 5008–
712 5027, doi: 10.1002/2016JA023700.
713
714 Wygant, J., Mozer, F., Temerin, M., Blake, J., Maynard, N., Singer, H., Smiddy, M., 1994.
715 Large amplitude electric and magnetic field signatures in the inner magnetosphere during

716 injection of 15 MeV electron drift echoes. *Geophys. Res. Lett.* 21 (16), 1739–1742.
717 https://doi.org/10.1029/94GL00375.
718